Impact of ΔF508 CFTR Mutation on Diaphragm Function During Acute Inflammation

Fatemeh Ostadan [1], Ekaterina Gusev [1], Feng Liang [1], Juan Bautista De Sanctis [3], Danuta Radzioch [1,4], Basil J Petrof [1,2]

1. Meakins-Christie Laboratories, Research Institute of the McGill University Health Centre, Montreal, Canada
2. Respiratory Division, Department of Medicine, McGill University, Montreal, Canada
3. Institute of Molecular and Translational Medicine, Faculty of Medicine and Dentistry, Palacky University, Olomouc, Czechia
4. Infectious Diseases and Immunity in Global Health, Research Institute of the McGill University Health Centre, Montreal, QC, Canada

Running Title: ΔF508 CFTR and Diaphragm Dysfunction with Inflammation

Corresponding author:
Basil J. Petrof, MD, FRCPC
Meakins Christie Laboratories
McGill University Health Centre - Research Institute
Montreal, Canada
E-mail: petrof.basil_j@mcgill.ca
Tel: (514) 934-1934, ext. 76172 (secretary), 76395 (office) or 76415 (lab)
Fax: (514) 933-3962
www.meakinsmcgill.com
www.basilpetrof.com

New & Noteworthy

The most common CFTR mutation in cystic fibrosis (CF), ΔF508 (DF-CFTR), was associated with signs of oxidative stress in the diaphragm without accompanying weakness or atrophy under baseline conditions. Lipopolysaccharide challenge to trigger acute systemic inflammation led to an exaggerated induction of oxidative stress and proteolytic pathways along with greater force loss in the DF-CFTR diaphragm compared to wild-type controls. This previously unrecognized vulnerability of the DF-CFTR diaphragm to systemic inflammation may predispose to respiratory muscle dysfunction in CF, particularly during acute infectious exacerbations.

Key words: Cystic fibrosis; Diaphragm muscle; Systemic inflammation; Oxidative stress; Muscle contractility

ABSTRACT

Background: Cystic fibrosis (CF) is caused by CFTR mutations and associated with skeletal muscle dysfunction. Prior work showed exaggerated inflammatory activation of proteolysis pathways in diaphragms of CFTR-null mice. However, effects of the more clinically relevant ΔF508 (DF-CFTR) mutation on diaphragm function are unknown.

Methods: Homozygous DF-CFTR mice ($Cftr^{tm1EUR}$) and wild-type (WT) littermates received intraperitoneal PBS or LPS (5 mg/kg). After 24 h, we evaluated diaphragm mass and fiber types; expression (mRNA) of cytokines (IL1β, IL6), the unfolded protein response (UPR), and proteolysis (ubiquitin-proteasome, autophagy-lysosome); calpain activity; oxidative stress markers (malondialdehyde, 3-nitrotyrosine); and ex vivo muscle contractility.

Results: Oxidative stress markers were higher in DF-CFTR diaphragms at baseline and in response to LPS. Atrogin1 and autophagy markers (LC3B, Gabarapl1) were more strongly induced by LPS in DF-CFTR. Expression of cytokines, UPR, and other proteolysis pathways (Murf1, calpain) were equivalent. Diaphragm mass, fiber diameter and fiber type proportions did not differ between groups. Contractile function did not differ at baseline, but only DF-CFTR diaphragms showed reduced force production after LPS.

Conclusion: During an acute inflammatory challenge, DF-CFTR diaphragms exhibit exaggerated oxidative stress and proteolysis signalling together with greater force loss. These findings support an increased vulnerability to diaphragm dysfunction linked to the DF-CFTR mutation.

INTRODUCTION

Cystic fibrosis (CF) is an autosomal recessive disease caused by loss-of-function mutations in the cystic fibrosis transmembrane conductance regulator (CFTR) protein. The primary function of CFTR is to act as an anion channel that transports chloride across the apical membrane of epithelial cells. However, CFTR is a pleiotropic protein which also significantly influences the transport of sodium, bicarbonate, glutathione, and other molecules (1-4). While progressive airway damage and recurrent pulmonary infections dominate the clinical picture in patients, CF is a disorder which affects multiple organ systems. Skeletal muscle is among the affected tissues, exhibiting atrophy and weakness in many patients (5). The presence of respiratory (eg, diaphragm) and non-respiratory muscle involvement by the disease is associated with increased morbidity as well as mortality (6).

The etiology of skeletal muscle dysfunction in CF is multifactorial, with secondary factors such as relative inactivity and impaired nutritional status playing a significant role in many patients (5). Some but not all studies have reported evidence for intrinsic physiologic defects of skeletal muscle (7, 8), possibly caused by defective CFTR function within the muscle fibers per se (9-12). In this regard, our group first demonstrated that CFTR is expressed at the mRNA transcript and protein levels in skeletal muscle fibers in vivo as well as in cultured myogenic cells (9). In both normal murine and human skeletal muscle, we reported for the first time that CFTR co-localises with Ca^{2+}-handling proteins in the sarcoplasmic reticulum, and in contrast to epithelial cells is only weakly detected at the cell surface membrane (9). Subsequent studies by others confirmed the presence and localisation of CFTR in skeletal muscle cells (11-13), but its precise role and the

84 consequences of CFTR mutations for skeletal muscle function under different physiologic
85 conditions remain poorly understood.

86 In previous work we showed that *Pseudomonas aeruginosa* lung infection in CFTR-null
87 mice triggered exaggerated induction of E3 ubiquitin ligases (Murf1 and Atrogin1)
88 associated with skeletal muscle proteolysis as well as contractile weakness in the
89 diaphragm (9). More recently, we observed that CFTR-null mice show magnified calpain
90 activity, along with greater ubiquitin-proteasome and autophagy-lysosome gene
91 upregulation, in the diaphragm during acute systemic inflammation induced by
92 lipopolysaccharide (LPS) injection (10). These data collectively suggest that in the face
93 of an acute inflammatory challenge which could be considered analogous to an acute
94 infectious exacerbation of CF disease, complete absence of CFTR is detrimental to
95 diaphragm function. However, whether similar abnormalities in diaphragm function occur
96 when CFTR is mutated to its most common and thus clinically relevant form, ΔF508 (DF-
97 CFTR), has not been addressed.

98 The DF-CFTR mutation destabilises the first nucleotide-binding domain of CFTR and
99 interferes with domain-domain interactions, leading to retention of the misfolded protein
100 in the endoplasmic reticulum (ER) and impeding its delivery to the epithelial cell surface
101 (14). Given the aberrant function of DF-CFTR in other cell types (15), it is plausible that
102 this mutation could be a significant contributor to skeletal muscle dysfunction in CF. In
103 addition, previous work has indicated the presence of chronic oxidative stress and
104 inflammation in CF compared to non-CF epithelial cells under basal conditions (16).
105 Accordingly, the principal objectives of the present study were to determine whether the

DF-CFTR mutation predisposes to exaggerated activation of cellular pathways previously linked to pathological muscle wasting and weakness (inflammation, oxidative stress, UPR/ER stress, proteolysis), and to directly assess contractile function of the diaphragm both at baseline and in response to an acute inflammatory stimulus.

MATERIALS AND METHODS

Animals

Mice heterozygous for the DF-CFTR mutation ($Cftr^{tm1EUR}$) on the C57BL/6J background were obtained from the Erasmus Medical Center and bred in-house to generate homozygous DF-CFTR mice and their wild-type littermates (WT-CFTR). Pups were genotyped at 3–4 weeks of age using DNA obtained by ear-punch biopsy, and CFTR status was confirmed by PCR following the established protocols for the Cftrtm1EUR allele (17, 18). Mice were housed under a 12-h light/dark cycle with corn-cob bedding (Anderson, Bestmonro, LA) and provided an NIH31-modified irradiated chow diet (Harlan Teklad, Indianapolis, IN).

At 13–16 weeks of age, mice were randomly assigned to receive either phosphate-buffered saline (PBS) or LPS via intraperitoneal injection. LPS derived from *Pseudomonas aeruginosa* (Sigma-Aldrich), a common pathogen in CF patients, was administered at a dose of 5 mg/kg as previously described (10). At 24 h post-injection, animals were anesthetized with isoflurane gas until loss of consciousness and then euthanized by cervical dislocation prior to collecting the diaphragm muscle. Due to the limited size of the diaphragm muscle tissue, not all assays could be performed on every

animal. All procedures were conducted in accordance with the guidelines of the Canadian Council on Animal Care and were approved by the McGill University Animal Care Committee.

Immunohistochemistry

Muscle samples were embedded in Cryomatrix (Thermo Scientific, USA), then snap-frozen in 2-methylbutane cooled with liquid nitrogen and stored at –80°C. Cryostat sections with 8 micrometer thickness were prepared and fixed in ice-cold acetone at –20°C for 10 min, followed by a 15-min air-dry. Sections were then blocked for 1 h at room temperature in the dark using Serum-Free Protein Block (Cat #X0909, Dako, USA). Overnight incubation at 4°C with primary antibodies targeting myosin heavy chain (MyHC) isoforms was performed, obtained from the Developmental Hybridoma Bank (USA); antibodies detected slow-twitch type I (clone BA-D5, 1:25 dilution), fast-twitch type IIa (clone SC-71, 1:300 dilution), and fast-twitch type IIb (clone BF-F3, 1:50 dilution) as we have previously described (10). Fibers that did not react with any of these antibodies were classified as type IIx by exclusion. After washing with PBS, the sections were incubated for 1 h at room temperature with secondary antibodies (from Invitrogen, USA) at a 1:500 dilution: Alexa Fluor 350 IgG2b (Cat #A21140), Alexa Fluor 488 IgG1 (Cat #A21121), and Alexa Fluor 555 IgM (Cat #A21426). All antibodies were diluted in Antibody Diluent Background Reducing Reagent (Cat #S3022, Dako, USA). Images were acquired using a Zeiss Axio Imager M2 microscope, and quantitative analysis of MyHC fiber type distribution and fiber size, assessed as Feret's minimal diameter to minimize errors from

oblique sectioning, was performed on at least 150 fibers per sample using ImageJ software as previously described (10).

Quantitative PCR (qPCR)

For quantitative PCR analysis, muscle samples were rapidly frozen in liquid nitrogen–cooled 2-methylbutane and stored at –80°C until processing. Total RNA was isolated using TRIzol reagent (Cat #15596018, Fisher Scientific, USA) with subsequent purification via a chloroform–isopropanol extraction protocol. One microgram of RNA was reverse transcribed into cDNA using random primers and the iScript RT-qPCR Supermix (Bio-Rad, USA). qPCR was then performed on 10 ng of cDNA in a reaction mixture that included 5 µL of 2x SYBR Green master mix (Cat #A25741, Applied Biosystems, USA) and 0.5 µL of a 10 µM primer mix. Amplification was carried out on a StepOne Plus Real-Time PCR System (Applied Biosystems, USA) for 40 cycles, consisting of a denaturation step at 95°C for 15 s followed by an annealing step at 60°C for 1 min, with all samples run at least in duplicate. Relative mRNA levels of target genes (UPR: Atf4, Edem1, Ddit3/Chop, Ppp1r15a/Gadd34, Xbp1s (spliced), and Hspa5/Bip; Pro-inflammatory cytokines: IL1β, IL6; Proteolysis: Murf1, Atrogin1, Lc3b, Gabarapl1, Bnip3) were quantified using the 2(-ΔΔCt) method and expressed as fold-change relative to the mean expression level in the PBS-treated WT-CFTR group. The Hprt1 gene served as the internal control, given its stable expression across experimental conditions and muscle types. Primer sequences for each target gene are listed in Online Supplemental Table 1, available at Figshare: https://doi.org/10.6084/m9.figshare.32413929.

Calpain Assay

Calpain activity was quantified using a fluorometric assay kit (Cat # ab65308, Abcam, USA) according to the manufacturer's instructions. Briefly, 10 mg of muscle tissue was homogenized on ice in 100 µL of extraction buffer to prevent calpain auto-activation. The homogenate was then centrifuged at 4°C for 5 min, and the supernatant was collected. Protein concentration was determined using a BCA Protein Assay Kit (Cat # 23225, Thermo Scientific, USA). Next, 50 µg of protein from the cytosolic fraction was incubated with 10 µL of a 10x Reaction Buffer and 5 µL of Calpain Substrate AcLLY-AFC at 37°C for 1 h. The assay was performed in duplicate in black, clear-bottom 96-well plates (Cat #3915, Corning, USA). Positive controls contained active calpain in extraction buffer. The cleavage of the substrate by calpain was measured using a microplate fluorometer (Tecan Infinite M200) with excitation/emission settings of 400/505 nm, and results were expressed as fluorescence per unit of muscle protein.

Markers of Oxidative Stress

Lipid and Protein Oxidation End Products

Lipid peroxidation was assessed fluorometrically by measuring thiobarbituric acid-reactive substances, which are end products of lipid peroxidation (19). Diaphragm tissue samples were homogenized and incubated with a reagent mixture containing 8.1% sodium dodecyl sulfate, 20% acetic acid, and 0.8% 2-thiobarbituric acid. After vortexing and incubation at 95°C for 1 h, butanol-pyridine was added at a 15:1 (v/v) ratio. The mixture was then shaken and centrifuged, and the resulting butanol-pyridine layer was fluorometrically analyzed at an excitation wavelength of 515 nm and emission at 552 nm

using an OptiPlate Perkin-Elmer system. Results were expressed as nanomoles of malondialdehyde (MDA) per milligram of protein, reflecting thiobarbituric acid-reactive species (20). For protein oxidation, the presence of 3-nitrotyrosine, a marker of oxidative and nitrosative stress, was quantified using an enzyme-linked immunosorbent assay (ELISA) with highly specific antibodies as we have previously described, with an assay sensitivity of 50 pg/mL (20). The antibodies used included mouse IgG monoclonal and polyclonal antibodies targeting nitrotyrosine, as well as polyclonal goat anti-rabbit IgG-peroxidase, all sourced from Upstate Biotechnology (Lake Placid, NY).

Dihydroethidium (DHE) Staining for Reactive Oxygen Species

Frozen muscle samples were embedded in Cryomatrix (Thermo Scientific, USA), and cryosectioned at 10 µm. Sections were allowed to equilibrate to room temperature for 10 min, then incubated in 5 µM DHE (Thermo Fisher) dissolved in PBS + 0.02 % Pluronic for 30 min at 37 °C in a light-protected, humid chamber as previously described (21). After two PBS washes, tissues were rinsed, and coverslipped with ProLong Gold. Fluorescence images were acquired on a Zeiss Axio Imager (excitation 530–560 nm; emission 590–620 nm) using identical exposure settings across all slides. Mean cytosolic fluorescence intensity was quantified in ≥6 random fields per section with ImageJ, background-subtracted, and averaged to yield one value per animal. Analyses were performed blinded to genotype and treatment.

Measurement of Isometric Contractile Force

Contractile force measurements of the diaphragm were performed as previously described (9). Briefly, diaphragm muscle was surgically excised immediately after animal sacrifice and placed into a chilled (4°C) and equilibrated (95% O_2–5%CO_2, pH 7.38) Krebs solution. From diaphragm, a muscle strip approximately 2 mm wide was dissected free, taking care to leave the central tendon and adjacent rib cage margins intact. The excised diaphragm strip was mounted into a jacketed tissue bath chamber filled with Krebs solution, using the 800A muscle apparatus (from Aurora Scientific). A thermoequilibration period of 15 min was observed before initiating contractile measurements at 23°C. After placing the muscle at optimal length, the force–frequency relationship was determined by sequential supramaximal stimulation for 1 s at 10, 30, 50, 100, and 150 Hz, with 2 min between each stimulation train. Fatigue resistance was assessed using repeated supramaximal tetanic contractions (200 ms trains) delivered for 180 s. The force data were acquired to computer at a sampling rate of 1000 Hz for later analysis. After completion of the above contractility studies, and before the muscles were removed from their baths, muscle length was measured with a microcaliper accurate to 0.1 mm. Muscle force was normalized to tissue cross-sectional area, which was determined by assuming a muscle density of 1.056 g/cm^3. Specific force (force/cross-sectional area) is expressed in Newtons/cm^2.

Statistics

Statistical analyses were conducted using GraphPad Prism (version 10.0 for macOS). Initially, all outcome measures were evaluated for normality using the Shapiro-Wilk test. For datasets that met the normality criteria, a two-way ANOVA test was performed with mouse strain (WT-CFTR vs. DF-CFTR) and treatment (PBS vs. LPS) as factors, followed by Tukey's post-hoc test for multiple comparisons to assess differences between group means. If the data did not meet normality assumptions, we employed a non-parametric Kruskal-Wallis test along with Dunn's post-hoc test. The result of the statistical analysis is provided as p-value. Outliers detected by the software were excluded from the analysis, and the sample size (n) for each group is provided in the corresponding figure legends. A significance level of $p<0.05$ (two-tailed) was used for all tests.

RESULTS

Initial body weight values at baseline were not different between groups (WT-CFTR: 26.08 ± 4.4 g, n=12; DF-CFTR: 24.16 ± 4.8 g, n=12). At 24 h after LPS administration, both WT-CFTR and DF-CFTR mice experienced significant weight loss of similar magnitude (Fig 1a), and the diaphragm muscle weight to overall body weight ratio remained stable in both groups (Fig 1b).

We next performed MyHC immunohistochemistry to identify slow-twitch (type I) and fast-twitch (types IIa, IIx, and IIb) muscle fibers in the diaphragm (Fig 2a). The relative percentages of the different MyHC-defined fiber types did not differ between WT-CFTR and DF-CFTR mice at baseline, and were unaffected by LPS administration in both

groups (Fig 2b). Mean fiber diameter for each muscle fiber subtype was also equivalent between the two mouse genotypes and unchanged by LPS treatment (Fig 2c).

UPR/ER stress, pro-inflammatory, and proteolysis pathways

Because DF-CFTR is misfolded and could potentially induce ER stress in the diaphragm, as well as the fact that inflammation can trigger ER stress signalling, we quantified transcript levels for genes associated with the unfolded protein response (UPR) (Fig. 3). There were no baseline differences between WT-CFTR and DF-CFTR mice in expression of the canonical UPR genes Atf4, Edem1, Ddit3/Chop, Ppp1r15a/Gadd34, Xbp1s (spliced), and Hspa5/Bip. In addition, none of these genes showed significantly altered expression at 24 h after LPS administration.

We next assessed transcript levels of classical pro-inflammatory genes and proteolysis pathways that are known to be associated with muscle wasting. The cytokines IL1β and IL6 (Fig 4a) did not show statistically significant differences between WT-CFTR and DF-CFTR groups under basal conditions. Following LPS treatment, both mouse genotypes demonstrated upregulation of IL1β and IL6 in the diaphragm, but these responses were not significantly different between the WT-CFTR and DF-CFTR groups.

There are 3 major proteolytic pathways closely linked to muscle wasting – the calpain, ubiquitin-proteasome, and autophagy systems. Baseline calpain activity was similar between WT-CFTR and DF-CFTR mice and remained unchanged after LPS treatment (Fig 4b). Transcript level measurements of the muscle-specific E3 ubiquitin ligases, Murf1

and Atrogin1, did not reveal baseline differences. However, LPS treatment significantly upregulated Murf1 in both genotypes, whereas Atrogin1 was only upregulated in the DF-CFTR diaphragm (Fig 4c). Similarly, assessment of the autophagy pathway showed equivalent levels of several prototypical markers (Lc3b, Gabarapl1, Bnip3) under basal conditions, but more pronounced responses to LPS for Lc3b and Gabarapl1 in the DF-CFTR group (Fig 4d).

Oxidative stress

Basal levels of MDA (Fig 5a) and 3-nitrotyrosine (Fig 5b), which are cumulative end-product markers of prior oxidative stress, were significantly elevated in DF-CFTR diaphragms compared to WT-CFTR controls. Following LPS administration, DF-CFTR mice exhibited a further significant increase in both MDA and 3-nitrotyrosine levels relative to their baseline as well as greater values in comparison to the LPS-treated WT-CFTR mice. DHE fluorescence intensity, which measures the instantaneous presence of reactive oxygen species, was similar between WT-CFTR and DF-CFTR diaphragms at baseline (Fig 5c), but showed a trend toward higher values in the DF-CFTR group after LPS administration ($p = 0.17$).

Diaphragm contractility

Ex vivo contractile function of the diaphragm was measured at baseline and in response to LPS treatment in the two mouse genotypes. Under basal conditions, there were no differences in maximum force production between WT-CFTR and DF-CFTR mouse diaphragms. However, only the DF-CFTR group demonstrated a significant reduction in maximum force-generating capacity of the diaphragm following LPS administration (Fig

6a). Ex vivo fatigue resistance of the diaphragm, expressed relative to the initial force value at the start of the fatigue protocol, did not differ between any of the groups (Fig 6b).

DISCUSSION

In the present investigation, we sought to determine whether the DF-CFTR mutation renders the diaphragm more vulnerable to muscle wasting and contractile dysfunction, either at baseline or in response to an acute systemic inflammatory stimulus. We found that DF-CFTR diaphragms exhibit evidence of higher basal oxidative and nitrosative stress (elevated MDA and 3-nitrotyrosine, respectively) compared with WT, and that these markers show a greater LPS-induced increase in DF-CFTR than in WT-CFTR mice. Furthermore, only DF-CFTR mice developed a significant reduction in maximal specific diaphragm force 24 h after LPS, despite preserved muscle mass, fiber size and fiber-type profile. This force loss was accompanied by a greater LPS-induced induction of several ubiquitin–proteasome and autophagy–lysosome system genes in DF-CFTR diaphragms, while calpain activity remained similar between genotypes. Canonical UPR transcripts did not differ significantly between groups at this time point. Taken together, these findings suggest that the DF-CFTR mutation promotes a redox- and proteostasis-altered milieu in the diaphragm that favors contractile dysfunction in the face of an acute inflammatory challenge.

Before discussing these findings in detail, several limitations of this study should be acknowledged. First, the induction of proteolysis signalling and other genes at the mRNA level does not prove the existence of increased protein degradation or other functional outcomes. Second, the mutation in our DF-CFTR mice is not myofiber-specific and thus other cell types within the muscle tissue besides the muscle fibers per se, could also be involved in the observed responses. Third, we focused exclusively on the diaphragm and

cannot determine whether these responses are diaphragm-specific or part of a more generalized skeletal muscle phenotype. Fourth, while LPS-induced endotoxemia creates an acute systemic inflammatory response designed to model an acute infectious exacerbation, this does not fully represent the fluctuating inflammatory burden found in many CF patients. Finally, measurements were restricted to a single post-LPS time point (24 h), which may have missed earlier transient responses or later structural changes, including delayed fiber atrophy or ER-stress activation. Although our study indicates the existence of several significant differences between wild-type and DF-CFTR mice following inflammatory challenge, ascertaining the kinetics and functional interplay between these findings will require additional experimentation at several time points in larger numbers of animals.

A central observation in our study is that DF-CFTR diaphragm weakness after LPS administration was associated with greater oxidative stress and activation of proteolytic pathways relative to WT animals. In contrast, we did not detect any significant genotype- or treatment-dependent differences in canonical ER stress/UPR markers at 24 h, suggesting that these pathways are not substantially activated at this time point and are unlikely to be major contributors to the force loss observed in DF-CFTR diaphragms. The combination of elevated basal MDA and 3-nitrotyrosine in DF-CFTR diaphragms, followed by a further LPS-induced surge in these markers, is consistent with a chronically pro-oxidant state that is unmasked or amplified by systemic inflammation. Similar patterns of oxidative injury and lipid dysregulation have been reported in CF airways and in CFTR-null and DF-CFTR mouse lungs, with elevated markers of lipid peroxidation and/or nitrosative stress accompanied by abnormal fatty-acid and sphingolipid profiles (16, 22-

24). In these systems, lipid-targeted interventions such as fenretinide, sphingosine-1-phosphate lyase inhibition, and the retinoid formulation LAU-7b, as well as CFTR corrector/antioxidant combinations, at least partly normalized lipid imbalances and, in some models, reduced MDA and nitrotyrosine levels (16, 20, 22, 25, 26).

The pattern of proteolytic pathway activation we observed is broadly consistent with prior work in CFTR-null models. Our group previously showed that complete CFTR absence in mice amplifies Murf1 and Atrogin1 induction and diaphragm weakness during *Pseudomonas aeruginosa* lung infection (9). Using the more easily quantifiable inflammatory stimulus of LPS, we also reported that CFTR-null mice develop greater activation of calpain, ubiquitin–proteasome, and autophagy–lysosome genes in diaphragm and limb muscles after LPS compared with WT mice (10). In combination with the findings of the current study, these observations collectively suggest that defects in CFTR function lower the threshold for proteostasis-associated functional impairment during an inflammatory challenge. These effects of CFTR mutations on skeletal muscle function and proteostasis may also be age-dependent. In this regard, Chen al al. recently reported that in old (18 mo) but not in young (4 mo) mice studied under basal conditions, DF-CFTR limb muscles demonstrated fiber atrophy, lower muscle twitch force, and reduced expression of autophagy and myogenesis genes in DF-CFTR compared to age-matched wild-type mice (11). These abnormalities were partly rescued by overexpressing CFTR in the muscle or treating mice with the CFTR corrector lumacaftor (VX-809) (11).

The precise physiological function of CFTR in skeletal muscle fibers is poorly understood. Cell type-specific differences in CFTR localization may help to account for distinct

consequences of the DF-CFTR mutation in skeletal muscle versus the more well characterized epithelial cell effects. For example, in airway and other epithelial cell types, CFTR resides predominantly at the apical surface membrane, where it mediates chloride and bicarbonate secretion and indirectly modulates sodium and glutathione transport (1, 3, 4). In epithelial cells, the DF-CFTR mutation destabilizes nucleotide-binding domain 1, impairs domain–domain interactions, and leads to misfolding and abnormal intracellular retention of CFTR in the ER (14, 27, 28). In addition to this abnormal sequestration of DF-CFTR in the ER, the mutation causes impaired channel gating and decreased stability of the protein at the cell surface membrane compared to wild-type CFTR (28-30).

In normal murine and human skeletal muscle, by contrast, CFTR is expressed at lower overall levels and is primarily localized to the sarcoplasmic reticulum and sarcotubular network, where it co-localizes with Ca2+-handling proteins and shows only weak staining at the surface (sarcolemmal) membrane (9, 13). Thus, in skeletal muscle fibers it appears that the "default" CFTR location is largely intracellular rather than at the cell surface. Accordingly, problems caused by DF-CFTR in skeletal muscle may be more related to a dysfunctional or unstable CFTR protein within the sarcoplasmic reticulum rather than abnormal CFTR sequestration as found in epithelial cells. We have speculated that one normal function of CFTR in skeletal muscle may be to permit chloride to act as a counter ion that restores the sarcoplasmic reticulum membrane potential during high rates of Ca2+ release and uptake (9). In support of this idea, we previously demonstrated exaggerated potassium-evoked Ca2+ transients originating from the sarcoplasmic reticulum in cultured myotubes derived from CFTR-null mice as well as in normal myotubes treated with a CFTR inhibitor (9).

Abnormalities of skeletal muscle metabolism have also been reported in both CF patients and pre-clinical models. Exercising CF patients demonstrated abnormal muscle bioenergetics and delayed phosphocreatine recovery on 31P-MRS, consistent with an intrinsic defect in muscle metabolism attributed to CFTR dysfunction (13, 31). In CFTR-null mice, defective intracellular transport of glucose transporter 4 (Glut4) has been reported (12). In skeletal muscle mitochondria from DF-CFTR mice, a reduced capacity for oxidative phosphorylation was observed (32). In CFTR-defective cells more broadly, impaired electron transport chain function has been associated with increases in reactive oxygen species (ROS) and lipid peroxidation (33, 34).

The diaphragm has a relatively high mitochondrial content, and both resting and contraction-related ROS production are greater in diaphragm than in many limb muscles (35, 36). In non-CF sepsis models, nitric oxide can combine with superoxide to form peroxynitrite, contributing to mitochondrial dysfunction and 3-nitrotyrosine formation (37, 38). In CF studies, abnormal glutathione transport, reduced antioxidant reserves, and elevated circulating oxidative markers, including MDA and 3-nitrotyrosine, have been observed even in clinically stable patients (23, 39-43). Several non-CF experimental paradigms have deliberately increased ROS and/or reactive nitrogen species, using exogenous oxidants, contraction-induced ROS, or inflammatory stimuli such as LPS, to determine the impact on contractile function. These studies showed that myofibrillar and Ca2+-handling proteins (including myosin, troponin, ryanodine receptors, and SERCA) can acquire carbonyl adducts, nitrotyrosine residues, and reversible thiol oxidation, which are associated with reduced maximal specific force, slowed cross-bridge kinetics, and greater fatigability (36, 38, 44). Upregulated ubiquitin-proteasome system driven

proteolysis can also degrade and disrupt the function of sarcomeric and Ca2+-handling proteins, and this phenomenon is associated with weakness that often precedes the presence of histologically defined muscle fiber atrophy (45, 46). On the other hand, protein degradation mechanisms such as autophagy can be protective against muscle atrophy and dysfunction by maintaining proteostasis through the elimination of defective proteins and organelles (47). The results of the present study do not allow us to ascertain whether the induction of ubiquitin-proteasome and autophagy signalling in the DF-CFTR diaphragm during acute systemic inflammation is harmful or beneficial for specific force production.

In summary, our results support the concept that CFTR is an important regulator of diaphragm muscle homeostasis under inflammatory conditions. Although previous work provides a correlative framework to help interpret our findings, additional validation studies will be required to establish causation between the observed oxidative stress/proteolysis signalling responses and force loss in DF-CFTR diaphragms, as well as to determine the specific sources and cellular targets of oxidative modification in DF-CFTR muscle fibers. Future work should also determine how CFTR-targeted therapies and antioxidants or proteostasis-modulating interventions might improve respiratory muscle resilience in CF patients.

ACKNOWLEDGMENTS

This study was supported by Cystic Fibrosis Canada award 3308.

SUPPLEMENTAL MATERIAL

Supplemental Table 1 is available at Figshare:

https://doi.org/10.6084/m9.figshare.32413929.

FIGURE LEGENDS

Figure 1. Body weight loss and diaphragm mass following LPS treatment. (a) Percentage change in body weight 24 h after intraperitoneal injection of PBS or LPS in WT and DF mice. (b) Diaphragm mass normalized to final body weight. Abbreviations: WT, wild-type CFTR; DF, ΔF508-CFTR; PBS, phosphate-buffered saline; LPS, lipopolysaccharide. Group means, individual animal data, and SD bars are shown. Statistical significance is indicated by asterisks above the comparison bars: **P < 0.01; ***P < 0.001 (overall group differences assessed by ANOVA).

Figure 2. CFTR genotype and LPS treatment do not affect myosin heavy chain phenotype or muscle fiber size in the diaphragm. (a) Representative immunostaining of myosin heavy chain (MyHC) type I (slow-twitch – blue), type IIa (fast-twitch oxidative – green), and type IIb (fast-twitch glycolytic - red) fibers of diaphragm muscle are shown; type IIx fibers are identified by exclusion. (b) Fiber type proportions and (c) Fiber size (Feret's diameter) are shown for the diaphragm at 24 h after PBS or LPS delivery. Abbreviations: WT, wild-type CFTR; DF, ΔF508-CFTR; PBS, phosphate-buffered saline; LPS, lipopolysaccharide. Group means, individual animal data, and SD bars are indicated.

Figure 3. CFTR genotype and LPS treatment do not affect canonical UPR transcripts in the diaphragm. Relative diaphragm mRNA levels of ER stress-UPR genes Atf4, Edem1, Ddit3/Chop, Ppp1r15a/Gadd34, Xbp1 (spliced), and Hspa5/Bip were quantified by qPCR 24 h after PBS or LPS delivery. All mRNA data are expressed as n-fold change relative to the mean WT-PBS level. Abbreviations: WT, wild-type CFTR; DF, ΔF508-CFTR; PBS, phosphate-buffered saline; LPS, lipopolysaccharide. Group means, individual animal data, and SD bars are illustrated.

Figure 4. Mutated CFTR is associated with greater proteolytic signaling in the diaphragm following LPS treatment. At 24 h after PBS or LPS delivery, results are shown for: (a) Pro-inflammatory cytokine transcripts IL1β and IL-6; (b) Calpain activity (RFU = relative fluorescence units; (c) Ubiquitin–proteasome system genes Murf1 and Atrogin1; and (d) Autophagy–lysosome system genes Lc3b, Gabarapl1, and Bnip3. All mRNA data are expressed as n-fold change relative to the mean WT-PBS level. Abbreviations: WT, wild-type CFTR; DF, ΔF508-CFTR; PBS, phosphate-buffered saline; LPS, lipopolysaccharide. Group means, individual animal data, and SD bars are shown. Statistical significance is indicated by asterisks above the comparison bars: *P < 0.05; **P < 0.01 (overall group differences assessed by ANOVA or Kruskal–Wallis, as appropriate).

Figure 5. Mutated CFTR is associated with greater basal and LPS-induced oxidative stress in the diaphragm. (a) Levels of malondialdehyde (MDA) expressed in nmol/mg of protein, (b) 3-nitrotyrosine expressed in ng/mg of protein, and (c) dihydroethidium expressed (DHE) as RFU=relative florescence units. Markers of oxidative stress were determined at 24 h after PBS or LPS delivery. Abbreviations: WT, wild-type CFTR; DF, ΔF508-CFTR; PBS, phosphate-buffered saline; LPS, lipopolysaccharide. Group means, individual animal data, and SD bars are shown. Statistical significance is indicated by asterisks above the comparison bars: *P < 0.05; **P < 0.01; ***P < 0.001; ****P < 0.0001; exact P values are shown where indicated (overall group differences assessed by ANOVA).

Figure 6. Mutated CFTR is associated with greater LPS-induced loss of diaphragmatic force production. (a) Maximal specific force values and (b) Percent initial force decline over time (fatigue resistance) of the diaphragm 24 h after PBS or LPS delivery. Abbreviations: WT, wild-type CFTR; DF, ΔF508-CFTR; PBS, phosphate-buffered saline; LPS, lipopolysaccharide. Group means, individual animal data, and SD bars are shown. Statistical significance is indicated by asterisks above the comparison bars: ***P < 0.001; ****P < 0.0001 (overall group differences assessed by ANOVA).

REFERENCES

1. Linsdell P, Hanrahan JW. Glutathione permeability of CFTR. Am J Physiol. 1998;275(1):C323-6.
2. Collawn JF, Lazrak A, Bebok Z, Matalon S. The CFTR and ENaC debate: how important is ENaC in CF lung disease? Am J Physiol Lung Cell Mol Physiol. 2012;302(11):L1141-6.
3. Mall MA, Mayer-Hamblett N, Rowe SM. Cystic Fibrosis: Emergence of Highly Effective Targeted Therapeutics and Potential Clinical Implications. Am J Respir Crit Care Med. 2020;201(10):1193-208.
4. Hanssens LS, Duchateau J, Casimir GJ. CFTR Protein: Not Just a Chloride Channel? Cells. 2021;10(11).
5. Gruet M, Troosters T, Verges S. Peripheral muscle abnormalities in cystic fibrosis: Etiology, clinical implications and response to therapeutic interventions. J Cyst Fibros. 2017;16(5):538-52.
6. Dassios T. Determinants of respiratory pump function in patients with cystic fibrosis. Paediatr Respir Rev. 2015;16(1):75-9.
7. Tomlinson OW, Barker AR, Fulford J, Wilson P, Shelley J, Oades PJ, et al. Skeletal muscle contributions to reduced fitness in cystic fibrosis youth. Front Pediatr. 2023;11:1211547.
8. Rodriguez-Miguelez P, Erickson ML, McCully KK, Harris RA. CrossTalk proposal: Skeletal muscle oxidative capacity is altered in patients with cystic fibrosis. J Physiol. 2017;595(5):1423-5.
9. Divangahi M, Balghi H, Danialou G, Comtois AS, Demoule A, Ernest S, et al. Lack of CFTR in skeletal muscle predisposes to muscle wasting and diaphragm muscle pump failure in cystic fibrosis mice. PLoS Genet. 2009;5(7):e1000586.
10. Gusev E, Liang F, Bhattarai S, Broering FE, Leduc-Gaudet JP, Hussain SN, et al. Characterization of skeletal muscle wasting pathways in diaphragm and limb muscles of cystic fibrosis mice. Am J Physiol Regul Integr Comp Physiol. 2022;322(6):R551-R61.
11. Chen Z, Xu J, Hu P, Du W, Chen J, Zhang X, et al. Defective Cystic Fibrosis Transmembrane Conductance Regulator Accelerates Skeletal Muscle Aging by Impairing Autophagy/Myogenesis. J Cachexia Sarcopenia Muscle. 2025;16(1):e13708.
12. Gu J, Zhang W, Wu L, Gu Y. CFTR Deficiency Affects Glucose Homeostasis via Regulating GLUT4 Plasma Membrane Transportation. Front Cell Dev Biol. 2021;9:630654.
13. Lamhonwah AM, Bear CE, Huan LJ, Kim Chiaw P, Ackerley CA, Tein I. Cystic fibrosis transmembrane conductance regulator in human muscle: Dysfunction causes abnormal metabolic recovery in exercise. Ann Neurol. 2010;67(6):802-8.
14. Du K, Sharma M, Lukacs GL. The DeltaF508 cystic fibrosis mutation impairs domain-domain interactions and arrests post-translational folding of CFTR. Nat Struct Mol Biol. 2005;12(1):17-25.
15. Trouve P, Ferec C, Genin E. The Interplay between the Unfolded Protein Response, Inflammation and Infection in Cystic Fibrosis. Cells. 2021;10(11).
16. Veltman M, De Sanctis JB, Stolarczyk M, Klymiuk N, Bahr A, Brouwer RW, et al. CFTR Correctors and Antioxidants Partially Normalize Lipid Imbalance but not Abnormal Basal Inflammatory Cytokine Profile in CF Bronchial Epithelial Cells. Front Physiol. 2021;12:619442.

17. French PJ, van Doorninck JH, Peters RH, Verbeek E, Ameen NA, Marino CR, et al. A delta F508 mutation in mouse cystic fibrosis transmembrane conductance regulator results in a temperature-sensitive processing defect in vivo. J Clin Invest. 1996;98(6):1304-12.
18. van Doorninck JH, French PJ, Verbeek E, Peters RH, Morreau H, Bijman J, et al. A mouse model for the cystic fibrosis delta F508 mutation. EMBO J. 1995;14(18):4403-11.
19. Ohkawa H, Ohishi N, Yagi K. Assay for lipid peroxides in animal tissues by thiobarbituric acid reaction. Anal Biochem. 1979;95(2):351-8.
20. Centorame A, Dumut DC, Youssef M, Ondra M, Kianicka I, Shah J, et al. Treatment With LAU-7b Complements CFTR Modulator Therapy by Improving Lung Physiology and Normalizing Lipid Imbalance Associated With CF Lung Disease. Front Pharmacol. 2022;13:876842.
21. Sakellariou GK, Vasilaki A, Palomero J, Kayani A, Zibrik L, McArdle A, et al. Studies of mitochondrial and nonmitochondrial sources implicate nicotinamide adenine dinucleotide phosphate oxidase(s) in the increased skeletal muscle superoxide generation that occurs during contractile activity. Antioxid Redox Signal. 2013;18(6):603-21.
22. Guilbault C, Wojewodka G, Saeed Z, Hajduch M, Matouk E, De Sanctis JB, et al. Cystic fibrosis fatty acid imbalance is linked to ceramide deficiency and corrected by fenretinide. Am J Respir Cell Mol Biol. 2009;41(1):100-6.
23. Moliteo E, Sciacca M, Palmeri A, Papale M, Manti S, Parisi GF, et al. Cystic Fibrosis and Oxidative Stress: The Role of CFTR. Molecules. 2022;27(16).
24. Scholte BJ, Horati H, Veltman M, Vreeken RJ, Garratt LW, Tiddens H, et al. Oxidative stress and abnormal bioactive lipids in early cystic fibrosis lung disease. J Cyst Fibros. 2019;18(6):781-9.
25. Veltman M, Stolarczyk M, Radzioch D, Wojewodka G, De Sanctis JB, Dik WA, et al. Correction of lung inflammation in a F508del CFTR murine cystic fibrosis model by the sphingosine-1-phosphate lyase inhibitor LX2931. Am J Physiol Lung Cell Mol Physiol. 2016;311(5):L1000-L14.
26. Wojewodka G, De Sanctis JB, Bernier J, Berube J, Ahlgren HG, Gruber J, et al. Candidate markers associated with the probability of future pulmonary exacerbations in cystic fibrosis patients. PLoS One. 2014;9(2):e88567.
27. Lewis HA, Buchanan SG, Burley SK, Conners K, Dickey M, Dorwart M, et al. Structure of nucleotide-binding domain 1 of the cystic fibrosis transmembrane conductance regulator. EMBO J. 2004;23(2):282-93.
28. Wang XR, Li C. Decoding F508del misfolding in cystic fibrosis. Biomolecules. 2014;4(2):498-509.
29. Okiyoneda T, Barriere H, Bagdany M, Rabeh WM, Du K, Hohfeld J, et al. Peripheral protein quality control removes unfolded CFTR from the plasma membrane. Science. 2010;329(5993):805-10.
30. Lukacs GL, Chang XB, Bear C, Kartner N, Mohamed A, Riordan JR, et al. The delta F508 mutation decreases the stability of cystic fibrosis transmembrane conductance regulator in the plasma membrane. Determination of functional half-lives on transfected cells. J Biol Chem. 1993;268(29):21592-8.
31. Wells GD, Wilkes DL, Schneiderman JE, Rayner T, Elmi M, Selvadurai H, et al. Skeletal muscle metabolism in cystic fibrosis and primary ciliary dyskinesia. Pediatr Res. 2011;69(1):40-5.

593 32. Lai N, Kummitha C, Drumm M, Hoppel C. Alterations of skeletal muscle bioenergetics
594 in a mouse with F508del mutation leading to a cystic fibrosis-like condition. Am J Physiol
595 Endocrinol Metab. 2019;317(2):E327-E36.
596 33. Atlante A, Favia M, Bobba A, Guerra L, Casavola V, Reshkin SJ. Characterization of
597 mitochondrial function in cells with impaired cystic fibrosis transmembrane conductance
598 regulator (CFTR) function. J Bioenerg Biomembr. 2016;48(3):197-210.
599 34. Patergnani S, Vitto VAM, Pinton P, Rimessi A. Mitochondrial Stress Responses and
600 "Mito-Inflammation" in Cystic Fibrosis. Front Pharmacol. 2020;11:581114.
601 35. Nethery D, DiMarco A, Stofan D, Supinski G. Sepsis increases contraction-related
602 generation of reactive oxygen species in the diaphragm. J Appl Physiol (1985). 1999;87(4):1279-
603 86.
604 36. Zuo L, Christofi FL, Wright VP, Liu CY, Merola AJ, Berliner LJ, et al. Intra- and
605 extracellular measurement of reactive oxygen species produced during heat stress in diaphragm
606 muscle. Am J Physiol Cell Physiol. 2000;279(4):C1058-66.
607 37. Boczkowski J, Lanone S, Ungureanu-Longrois D, Danialou G, Fournier T, Aubier M.
608 Induction of diaphragmatic nitric oxide synthase after endotoxin administration in rats: role on
609 diaphragmatic contractile dysfunction. J Clin Invest. 1996;98(7):1550-9.
610 38. Boczkowski J, Lisdero CL, Lanone S, Samb A, Carreras MC, Boveris A, et al.
611 Endogenous peroxynitrite mediates mitochondrial dysfunction in rat diaphragm during
612 endotoxemia. FASEB J. 1999;13(12):1637-46.
613 39. Antus B, Drozdovszky O, Barta I, Kelemen K. Comparison of Airway and Systemic
614 Malondialdehyde Levels for Assessment of Oxidative Stress in Cystic Fibrosis. Lung.
615 2015;193(4):597-604.
616 40. Balint B, Kharitonov SA, Hanazawa T, Donnelly LE, Shah PL, Hodson ME, et al.
617 Increased nitrotyrosine in exhaled breath condensate in cystic fibrosis. Eur Respir J.
618 2001;17(6):1201-7.
619 41. Causer AJ, Shute JK, Cummings MH, Shepherd AI, Gruet M, Costello JT, et al.
620 Circulating biomarkers of antioxidant status and oxidative stress in people with cystic fibrosis: A
621 systematic review and meta-analysis. Redox Biol. 2020;32:101436.
622 42. Galiniak S, Molon M, Rachel M. Links between Disease Severity, Bacterial Infections
623 and Oxidative Stress in Cystic Fibrosis. Antioxidants (Basel). 2022;11(5).
624 43. Gao L, Kim KJ, Yankaskas JR, Forman HJ. Abnormal glutathione transport in cystic
625 fibrosis airway epithelia. Am J Physiol. 1999;277(1):L113-8.
626 44. Powers SK, Ji LL, Kavazis AN, Jackson MJ. Reactive oxygen species: impact on skeletal
627 muscle. Compr Physiol. 2011;1(2):941-69.
628 45. Friedrich O, Reid MB, Van den Berghe G, Vanhorebeek I, Hermans G, Rich MM, et al.
629 The Sick and the Weak: Neuropathies/Myopathies in the Critically Ill. Physiol Rev.
630 2015;95(3):1025-109.
631 46. Marusic U, Narici M, Simunic B, Pisot R, Ritzmann R. Nonuniform loss of muscle
632 strength and atrophy during bed rest: a systematic review. J Appl Physiol (1985).
633 2021;131(1):194-206.
634 47. Masiero E, Agatea L, Mammucari C, Blaauw B, Loro E, Komatsu M, et al. Autophagy is
635 required to maintain muscle mass. Cell Metab. 2009;10(6):507-15.
636

637

FIGURE 1

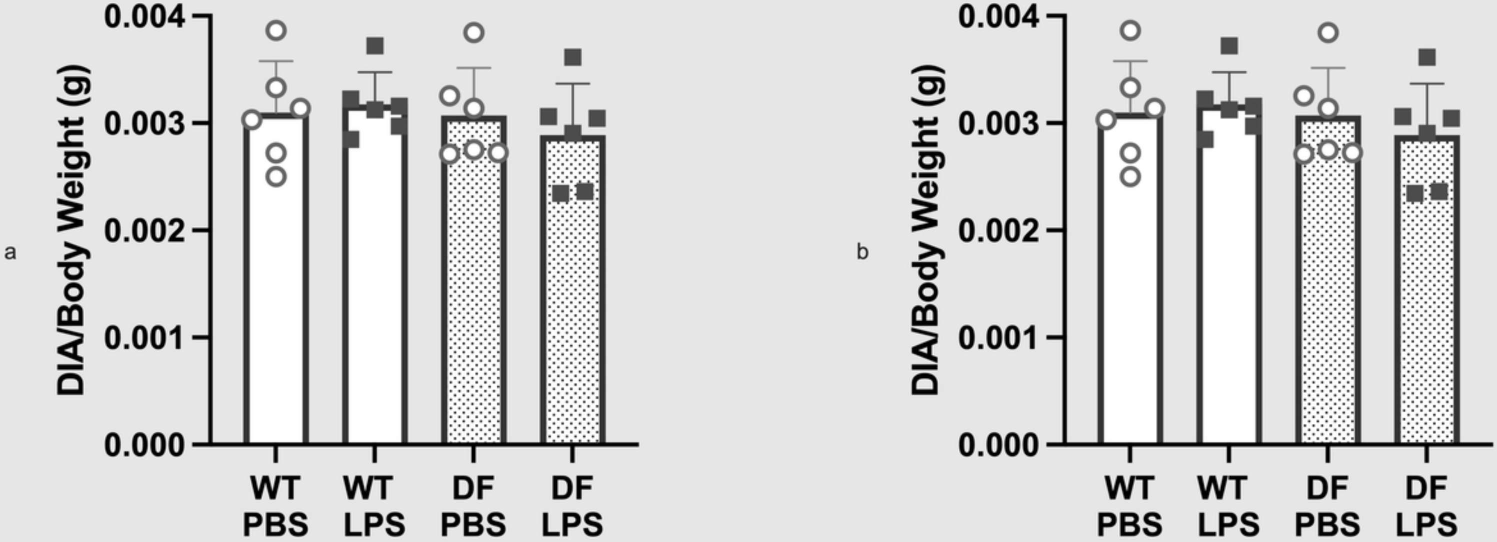

Figure 1. Body weight loss and diaphragm mass following LPS treatment. (a) Percentage change in body weight 24 h after intraperitoneal injection of PBS or LPS in WT and DF mice. (b) Diaphragm mass normalized to final body weight. Abbreviations: WT, wild-type CFTR; DF, ΔF508-CFTR; PBS, phosphate-buffered saline; LPS, lipopolysaccharide. Group means, individual animal data, and SD bars are shown. Statistical significance is indicated by asterisks above the comparison bars: **$P < 0.01$; ***$P < 0.001$ (overall group differences assessed by ANOVA).

FIGURE 2

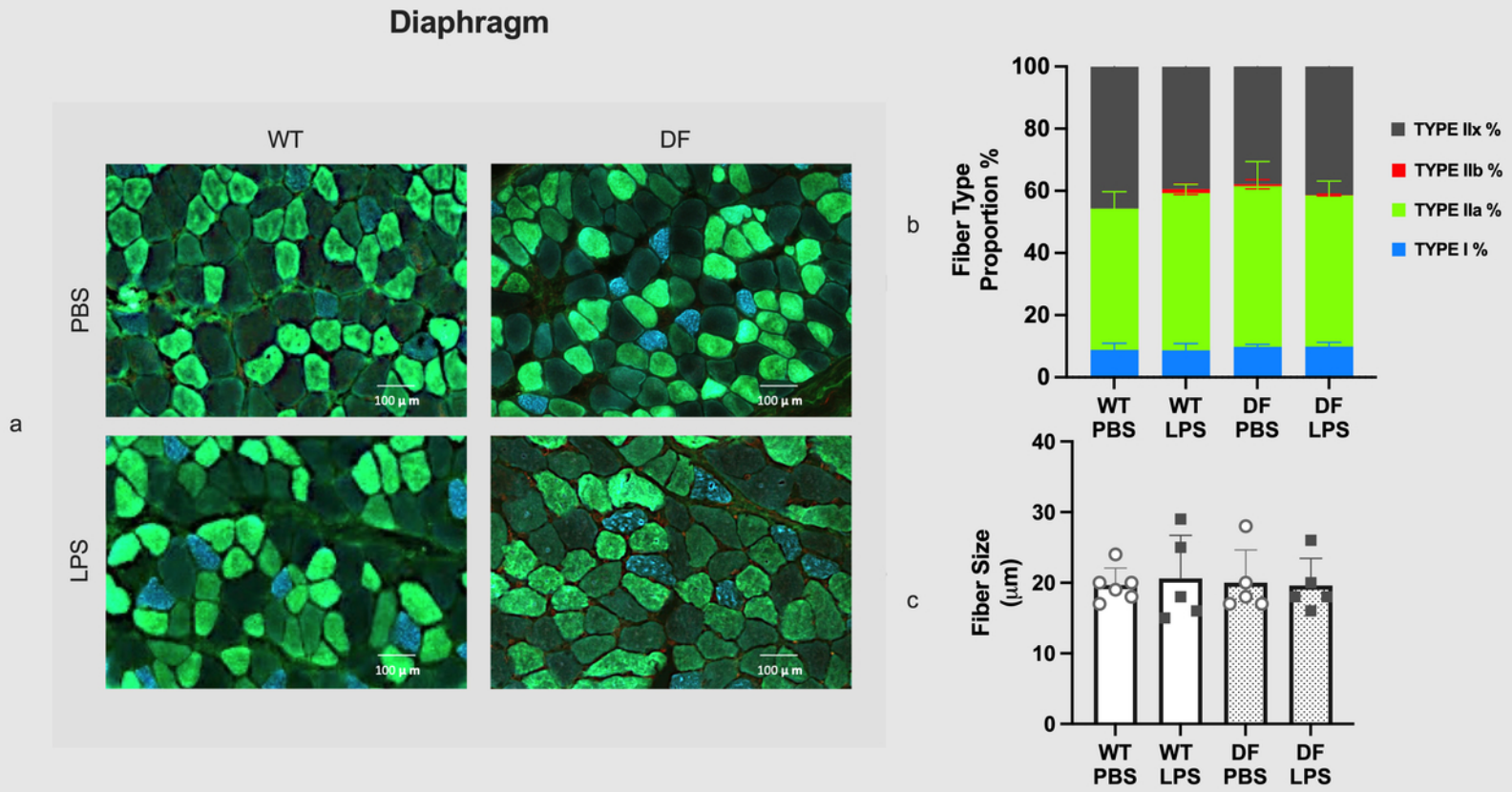

Figure 2. CFTR genotype and LPS treatment do not affect myosin heavy chain phenotype or muscle fiber size in the diaphragm. (a) Representative immunostaining of myosin heavy chain (MyHC) type I (slow-twitch – blue), type IIa (fast-twitch oxidative – green), and type IIb (fast-twitch glycolytic - red) fibers of diaphragm muscle are shown; type IIx fibers are identified by exclusion. (b) Fiber type proportions and (c) Fiber size (Feret's diameter) are shown for the diaphragm at 24 h after PBS or LPS delivery. Abbreviations: WT, wild-type CFTR; DF, ΔF508-CFTR; PBS, phosphate-buffered saline; LPS, lipopolysaccharide. Group means, individual animal data, and SD bars are indicated.

FIGURE 3

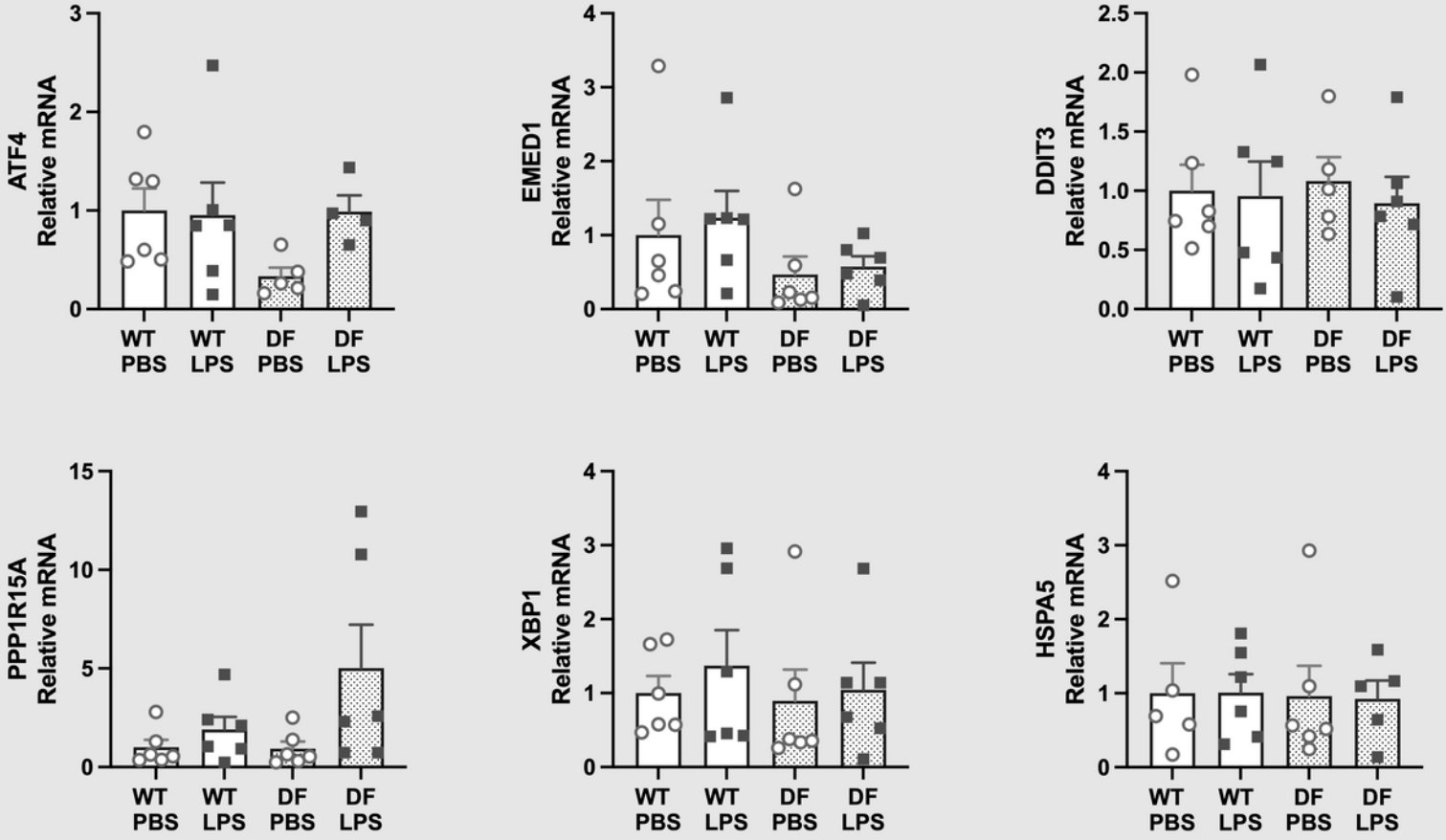

Figure 3. CFTR genotype and LPS treatment do not affect canonical UPR transcripts in the diaphragm. Relative diaphragm mRNA levels of ER stress-UPR genes Atf4, Edem1, Ddit3/Chop, Ppp1r15a/Gadd34, Xbp1 (spliced), and Hspa5/Bip were quantified by qPCR 24 h after PBS or LPS delivery. All mRNA data are expressed as n-fold change relative to the mean WT-PBS level. Abbreviations: WT, wild-type CFTR; DF, ΔF508-CFTR; PBS, phosphate-buffered saline; LPS, lipopolysaccharide. Group means, individual animal data, and SD bars are illustrated.

FIGURE 4

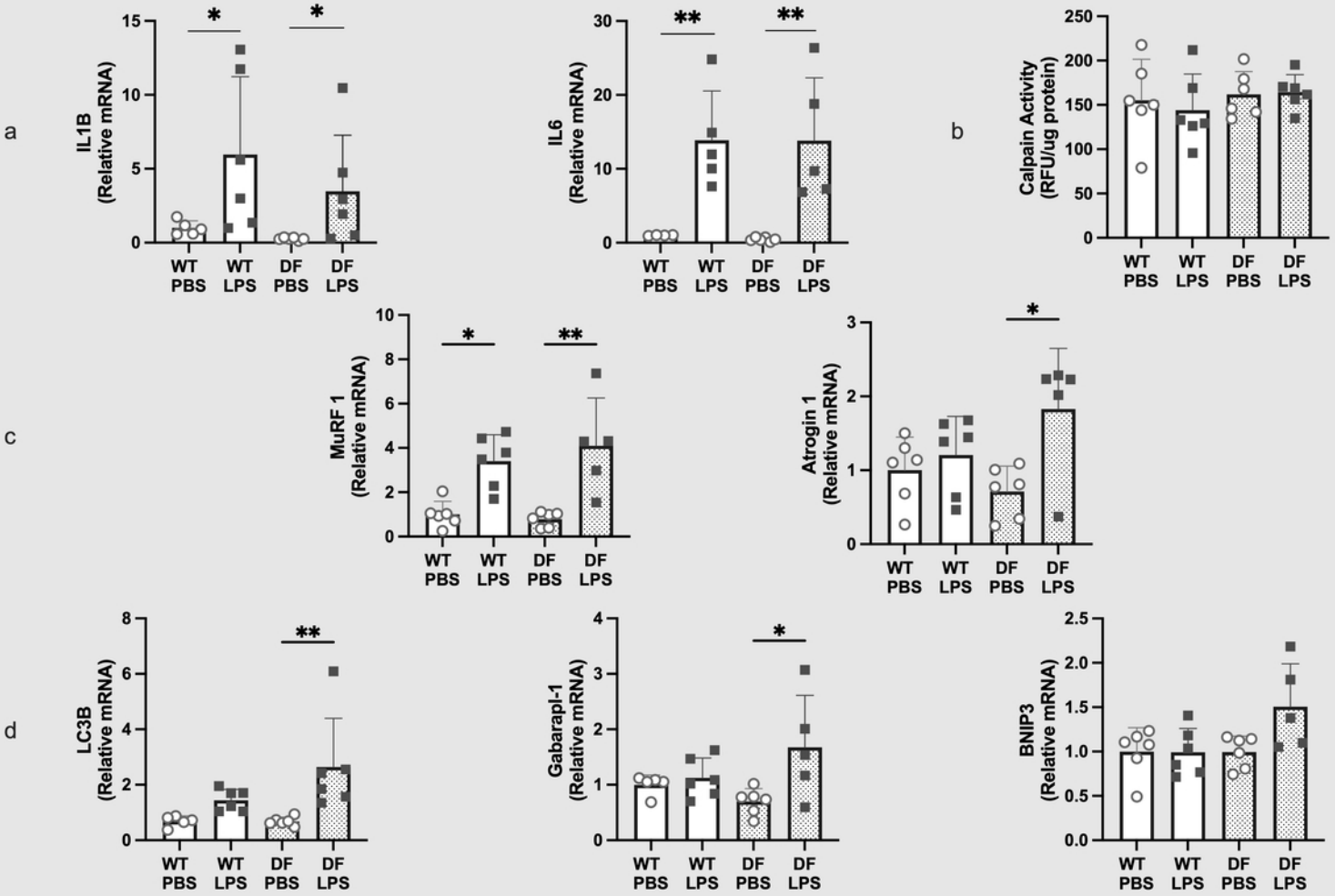

Figure 4. Mutated CFTR is associated with greater proteolytic signaling in the diaphragm following LPS treatment. At 24 h after PBS or LPS delivery, results are shown for: (a) Pro-inflammatory cytokine transcripts IL1β and IL-6; (b) Calpain activity (RFU = relative fluorescence units; (c) Ubiquitin–proteasome system genes Murf1 and Atrogin1; and (d) Autophagy–lysosome system genes Lc3b, Gabarapl1, and Bnip3. All mRNA data are expressed as n-fold change relative to the mean WT-PBS level. Abbreviations: WT, wild-type CFTR; DF, ΔF508-CFTR; PBS, phosphate-buffered saline; LPS, lipopolysaccharide. Group means, individual animal data, and SD bars are shown. Statistical significance is indicated by asterisks above the comparison bars: *P < 0.05; **P < 0.01 (overall group differences assessed by ANOVA or Kruskal–Wallis, as appropriate).

FIGURE 5

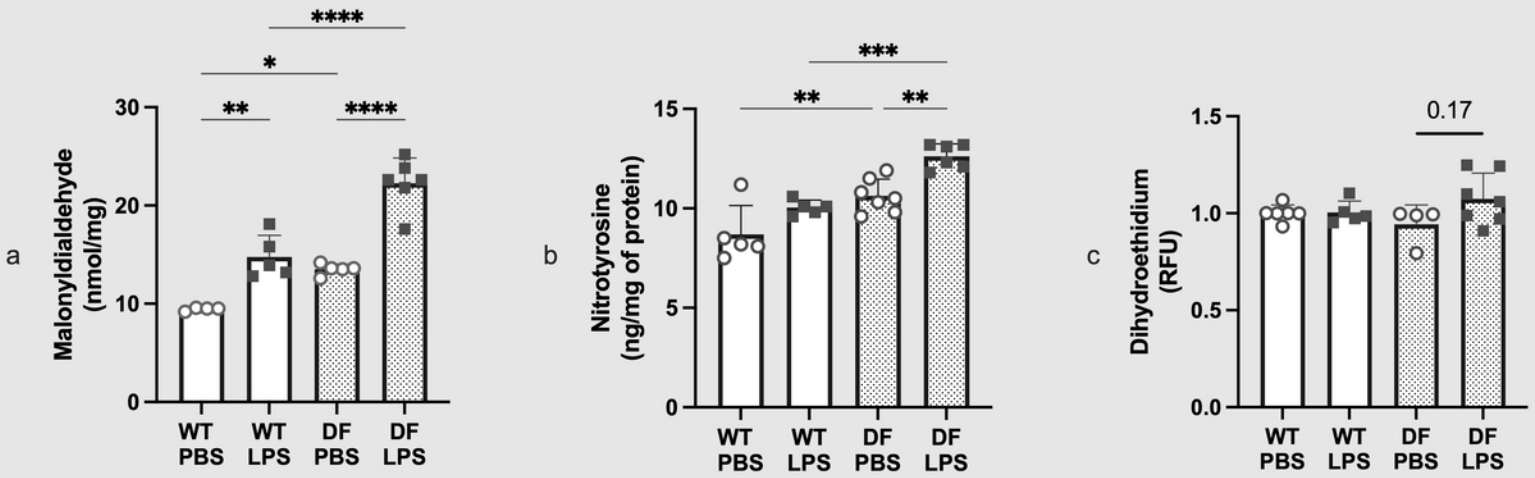

Figure 5. Mutated CFTR is associated with greater basal and LPS-induced oxidative stress in the diaphragm. (a) Levels of malondialdehyde (MDA) expressed in nmol/mg of protein, (b) 3-nitrotyrosine expressed in ng/mg of protein, and (c) dihydroethidium expressed (DHE) as RFU=relative florescence units. Markers of oxidative stress were determined at 24 h after PBS or LPS delivery. Abbreviations: WT, wild-type CFTR; DF, ΔF508-CFTR; PBS, phosphate-buffered saline; LPS, lipopolysaccharide. Group means, individual animal data, and SD bars are shown. Statistical significance is indicated by asterisks above the comparison bars: *P < 0.05; **P < 0.01; ***P < 0.001; ****P < 0.0001; exact P values are shown where indicated (overall group differences assessed by ANOVA).

FIGURE 6

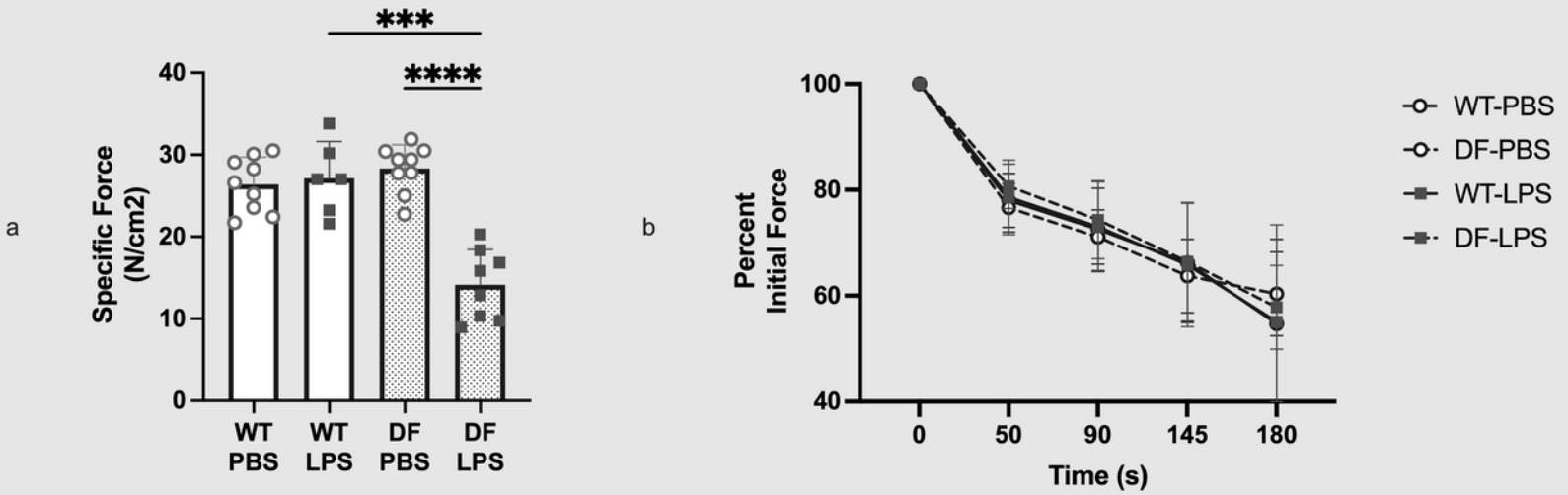

Figure 6. Mutated CFTR is associated with greater LPS-induced loss of diaphragmatic force production. (a) Maximal specific force values and (b) Percent initial force decline over time (fatigue resistance) of the diaphragm 24 h after PBS or LPS delivery. Abbreviations: WT, wild-type CFTR; DF, ΔF508-CFTR; PBS, phosphate-buffered saline; LPS, lipopolysaccharide. Group means, individual animal data, and SD bars are shown. Statistical significance is indicated by asterisks above the comparison bars: ***P < 0.001; ****P < 0.0001 (overall group differences assessed by ANOVA).